Chemosphere 268 (2021) 129363

Contents lists available at ScienceDirect

Chemosphere

journal homepage: www.elsevier.com/locate/chemosphere

Magnetic seeding coagulation: Effect of Al species and magnetic particles on coagulation efficiency, residual Al, and floc properties

Miao Lv [a], Dongyi Li [b], Zhaohan Zhang [a, **], Bruce E. Logan [c], Jan Peter van der Hoek [d], Muchen Sun [a], Fan Chen [e], Yujie Feng [a, *]

[a] State Key Laboratory of Urban Water Resource and Environment, School of Environment, Harbin Institute of Technology, Harbin, 150090, China
[b] School of Environmental Science and Engineering, Tianjin University, No. 92 Weijin Road, Nankai District, Tianjin, 300072, China
[c] Department of Civil and Environmental Engineering, Penn State University, 212 Sackett Building, University Park, PA, 16802, United States
[d] Department of Water Management, Delft University of Technology, PO Box 5048, 2600, GA, Delft, the Netherlands
[e] School of Ecology and Environment, Northwestern Polytechnical University, Xi'an, 710129, China

HIGHLIGHTS

- Compositing MPs to $AlCl_3$ improved primary cluster size and their aggregation.
- MPs-Al_{13}-DOM clusters facilitated DOC removal and residual Al reduction.
- Significant interaction for turbidity removal was observed between MPs and Al_{30}.
- Interactions between Al species and MPs guide the application of an effective MSC process.

GRAPHICAL ABSTRACT

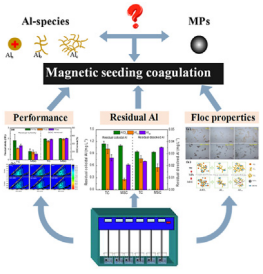

ARTICLE INFO

Article history:
Received 25 September 2020
Received in revised form
1 December 2020
Accepted 15 December 2020
Available online 17 December 2020

Handling Editor: E. Brillas

Keywords:
Magnetic particles
Coagulation
Al species
Response surface methodology
Floc properties

ABSTRACT

Magnetic seeding coagulation (MSC) process has been used to accelerate flocs sedimentation with an applied magnetic field, offering large handling capacity and low energy consumption. The interactions of three typical Al species, aluminum chloride ($AlCl_3$), $Al_{13}O_4(OH)_{24}^{7+}$ polymer (Al_{13}), and $(AlO_4)_2Al_{28}(OH)_{56}^{18+}$ polymer (Al_{30}), with magnetic particles (MPs) were examined to clarify the MSC process. In traditional coagulation (TC) process, the aggregation of primary Al_a-dissolved organic matter (DOM) complexes with in-situ-formed polynuclear species generated a large average floc size (226 μm), which was proved to be efficient for DOC removal (52.6%). The weak connections between dissolved Al_a-DOM complexes and MPs led to the negligible changes of dissolved Al after seeding with MPs in $AlCl_3$. A significant interaction between MPs and Al_{13} was observed, in which the MPs-Al_{13}-DOM complexes were proposed to be responsible for the significant improvement of DOC removal (from 47% to 52%) and residual total Al reduction (from 1.05 to 0.27 mg Al L^{-1}) with MPs addition. Al_{30} produced a lower floc fractal dimension ($D_f = 1.88$) than $AlCl_3$ (2.08) and Al_{13} (1.99) in the TC process, whereas its floc strength (70.9%) and floc recovery (38.5%) were higher than the others. Although more detached fragments were produced with MPs addition, the effective sedimentation of these fragments with the applied magnetic field led to the decrease of residual turbidity and colloidal Al in Al_{30}. The dependence of coagulation behavior to MPs and different Al species can be applied to guide the application of an effective MSC process.

* Corresponding author.
** Corresponding author.
E-mail addresses: hitzzh@hit.edu.cn (Z. Zhang), yujief@hit.edu.cn (Y. Feng).

https://doi.org/10.1016/j.chemosphere.2020.129363
0045-6535/

1. Introduction

Coagulation processes are widely used in water and wastewater treatment for the removal of colloidal particles, phosphorus, heavy metals, and organic matter due to their simplicity, cost-efficiency, and upgradeability (Ibarra-Rodríguez et al., 2017; Su et al., 2017; Liu et al., 2019). Aggregating colloids into large flocs in the coagulation process is generally susceptible to the fluctuation of operating conditions, which may lead to elevated concentrations of residual metal ions in treated water (Xu et al., 2010). Many researchers have confirmed the detrimental effect of residual metal ions on human health, such as the Alzheimer's disease resulting from high residual Al (Gauthier et al., 2000). Thus, there remains a need for producing stable flocs and improving their effective separation in water treatment processes. Increasing floc settling rates is always desirable, because a faster settling velocity can enable the use of smaller hydraulic retention times for water clarification and therefore smaller tank sizes. Larger settling tanks could increase capital and operational costs, especially in some cold areas where the settling basins should be placed in a heated building (Lapointe and Barbeau 2018). Therefore, methods of promoting the stable growth and rapid sedimentation of flocs can help to improve coagulation treatment efficiency and reduce the overall costs.

Particles present in high-turbidity water can provide increased floc nucleating sites and collisions for the formation of larger flocs than that possible in low-turbidity water (Yao et al., 2014). Adding particles with specific physical and chemical properties into the water could therefore benefit floc aggregation and coagulation performance. For instance, combining diatomite with polyaluminum chloride (PACl) produced settleable flocs with greater density, size, and strength resulting in improved removal of natural organic matter (NOM) and heavy metals from a slightly polluted algae-containing surface water (Wu et al., 2011). In the enhanced coagulation process with ferric ions and calcite for high-arsenic water treatment, small arsenic-borne coagulants coating on the calcite surfaces increased the settling rate of the particles (Song et al., 2006). Many different types of particles have been added to aid coagulation performance, including carbon nanotubes (Simate et al., 2012), magnetic particles (MPs) (Zhang et al., 2012), zeolites (Liao et al., 2016), bentonite (Ferhat et al., 2016), silica (Xue et al., 2016), and manganese dioxide (Huangfu et al., 2017). However, these methods not only required large quantities of materials but also produced a considerable amount of sludge, increasing the costs for the subsequent disposal of potentially hazardous sludges.

Magnetic seeding coagulation (MSC) is a newly emerging process where MPs are added to coagulate with other particles to form magnetic flocs with improved settability (Lv et al., 2019). Many studies have confirmed the effective recovery of MPs from flocs with an applied magnetic field (Xu et al., 2011a; Mandel et al., 2013), leading to a reduced volume of sludge with MPs addition compared to the other types of particles. The MSC process has also attracted great attention for offering advantages of higher contaminants removal, larger handling capacity, less residual metal ions in solution, and lower energy consumption than traditional coagulation (TC) processes (Ambashta and Sillanpää 2010). Jiang et al. (2010) synthesized a composite coagulant by combining Fe_3O_4 with polyferric chloride (PFC), which improved coagulation efficiency as shown by higher *Microcystis aeruginosa* removal and a slight pH dependence compared to adding only PFC (2010). Wan et al. (2011) reported that the dosage of polyaluminum chloride (PACl) when combined with magnetic seeds could be reduced by 83% compared to only PACl addition, as the magnetic seeds improved aggregation and precipitation of nanoparticles from the backside grinding wastewater. However, the previous studies were limited to the preparation and application of novel magnetic coagulants, focusing on their optimal operating conditions for contaminants removal. Very few studies have been conducted to investigate how MPs interact with coagulants during the MSC process. Zhang et al. (2012) proposed a plausible structure based on an Al species-nanoparticles cluster, which could have contributed to the unique properties of magnetic polyaluminium chloride (MPACl). The different types of Al species coexisted in the PACl, interactions between MPs and these different Al species are still not clear, and thus need further investigation.

Al-based coagulants are the most widely used materials in the coagulation process and the distribution of hydrolyzed Al species is generally recognized to be vital for the coagulation behavior (Yang et al., 2010; Hu et al., 2012). The hydrolyzed Al species can be divided into monomeric species (Al_a), intermediate polymer species (Al_b), and higher polymers with colloidal or solid species (Al_c) (Lee et al., 2012; Shirasaki et al., 2016). Al_a is mainly composed of monomer (Al^{3+}, $Al(OH)^{2+}$, $Al(OH)_2^+$) dimer ($Al_2(OH)_2^{4+}$), trimer ($Al_3(OH)_4^{5+}$) and some small polymers, which normally have small molecular weights (MWs) of <1 kDa, and a high charge per Al (Yan et al., 2007). Al_b has represented polymers with MWs in the range of 1 kDa−3 kDa, and Al_c represents large polymers with MWs larger than 3 kDa (Duan et al., 2014). Understanding the corresponding coagulation behaviors of different Al species with MPs is necessary for a more thorough MSC process analysis. Al_{13} and Al_{30} are regarded as efficient coagulation species due to their strong charge neutralization capability, high structural stability, and nano-sized effects (Ye et al., 2013). Therefore, understanding the interactive effects between MPs and these different hydrolyzed Al species is essential for researchers to gain an insight into the MSC process for pollutants removal.

In this study, different combinations of MPs and Al species were used in the MSC process to investigate the variation of coagulation performance and the corresponding interaction mechanisms. The specific objectives were to (i) visualize the mutual interaction between Al species and MPs for pollutants removal using the response surface methodology (RSM); (ii) investigate the effect of Al species and MPs on coagulation efficiency, residual Al and floc properties; and (iii) elucidate the interaction mechanism between MPs and Al species.

2. Materials and methods

2.1. Chemicals and synthetic water

Aluminum chloride ($AlCl_3 \cdot 6H_2O$), sodium hydroxide (NaOH), sodium sulfate (Na_2SO_4), barium chloride ($BaCl_2$), sodium bicarbonate ($NaHCO_3$), and kaolin power were obtained from the Sinopharm Chemical Reagent Co., Ltd. (Beijing, China). MPs (99.5% purity) were purchased from Beijing DK nano technology Co., Ltd. (Beijing, China), and the detailed characterization of MPs refers to the previous study (Lv et al., 2019). Ferron ($C_9H_6INO_4S$), 1,10-phenanthroline ($C_{12}H_8N_2$), hydroxylammonium chloride ($NH_2OH \cdot HCl$), hydrochloric acid (HCl), and aluminum powder (Al) were purchased from Sigma-Aldrich (St. Louis, Missouri, USA) and used for determining the distribution of Al species. All chemicals were of analytical grade and used as received without further purification.

Humic acid (HA, Sigma-Aldrich, USA)-Kaolin synthetic water was used as raw water to provide consistent and reproducible samples throughout the tests. HA stock solutions were prepared by dissolving 1.0 g HA in 1 L deionized water which contained 4.2 g $NaHCO_3$. The kaolin stock solution was prepared by dispersing 10.0 g Kaolin in 1 L deionized water with 3 h of vigorous stirring and then collecting the supernatant after settling for 1 h. HA (10 mL) and kaolin (5 mL) stock solutions were mixed with tap

water (1 L) to provide the raw water with a DOC of 6.8–7.5 mg L^{-1}, UV_{254} of 0.365–0.380 cm^{-1}, and pH of 7.3–7.5.

2.2. Preparation of Al-species and MPs-Al species

Three Al-based coagulants ($AlCl_3 \cdot 6H_2O$, Al_{13}, and Al_{30}), were selected to evaluate their coagulation behaviors in both MSC and TC processes. $AlCl_3 \cdot 6H_2O$ was prepared by directly dissolving 2.4143 g $AlCl_3 \cdot 6H_2O$ in 100 mL deionized water. The preparation of Al_{13} was carried out by the SO_4^{2-}/Ba^{2+} displacement method from the PACl with a basicity of 2.0 (PACl2.0), which was synthesized by the based titration method (Gao et al., 2009). The Al_{30} was prepared by high-temperature curing and purified by the SO_4^{2-}/Ba^{2+} precipitation method (Feng et al., 2015). Detailed descriptions are presented in the Supplementary Material. The MPs-Al species were synthesized by ultrasonic mixing MPs with $AlCl_3 \cdot 6H_2O$, Al_{13}, and Al_{30} at a fixed ratio for 30 min and blending in a shaker for 12 h. The Al species distributions of coagulants are presented in Table SM-1.

2.3. Design of jar tests

Coagulation experiments were performed on a program-controlled jar test apparatus with six paddles (ZR4-6, Zhongrun Water Industry Technology Development Co. Ltd., China). Central composited design (CCD) and response surface methodology (RSM) (Design Expert 8.0.6 software) were applied in the experimental design and mathematical modeling to investigate the influence and interaction of Al species and MPs. Preliminary experiments were conducted to determine the extreme values and obtain a narrower and more effective range of Al species dosages (Fig. SM-1). Al-species dosage (X_1) and MPs dosage (X_2) were selected as two independent variables, and their levels in coded and actual values are presented in Table SM-2. The experimental design matrix and two responses, turbidity removal (Y_1) and DOC removal (Y_2), are given in Table SM-3. The CCD was conducted with 20 experiments, including two replicates of four factorial points and four axial (star) points corresponding to the alpha value (0.5) and four replicates of center points. The mathematical models of turbidity and DOC removal rate were employed to assess the combined effects of these variables. Diagnostic checking test based on the variance analysis (ANOVA) was used to evaluate the adequacy of the proposed model. The optimum region was identified on the three-dimensional plots and their respective contour plots based on the response variables in an overlay plot.

Correlations between MPs, Al species, and coagulation behavior were evaluated at the optimized conditions during MSC and TC jar tests. For the coagulation procedure, the samples were mixed rapidly at 200 rpm for 2 min, stirred slowly at 50 rpm for 15 min, and settled for 30 min by gravity or by 5 min residence time on a cubic permanent magnet (0.5 T). Then, 100 mL supernatant was collected from approximately 3 cm below the top surface to analyze the residual pollutants.

2.4. Characterization of floc size, strength and fractal structure

The dynamic floc size in real-time was measured by a laser diffraction instrument (Mastersizer 2000; Malvern, UK). When the coagulation process proceeded, the flocs were transported by a peristaltic pump (BT100-2 J, Longer, China), monitored through the optical unit of the instrument, and automatically recorded every 30 s. The coagulation procedure for testing flocs was carried out as follows: rapid mixing at 200 rpm for 2 min, flocs growing phase at 50 rpm for 15 min, flocs breakage period at 200 rpm for 5 min and flocs regrowth phase at 50 rpm for 15 min. The floc strength factor (S_f) and recovery factor (R_f) were used to compare the breakage resistances and regrowth properties of the flocs using:

$$S_f = \frac{d_b}{d_i} \times 100\% \quad (1)$$

$$R_f = \frac{d_r - d_b}{d_i - d_b} \times 100\% \quad (2)$$

where d_i, d_b, and d_r are the average floc size (d_{50}) of the initial steady stage, breakage period and flocs regrowth phase. The fractal dimension (D_f) represents the structure of the flocs, which is determined by the relationship between light intensity (I) and scatter vector (Q) shown as follows (Lin et al., 2008; Cao et al., 2015):

$$I \propto Q^{-D_f} \quad (3)$$

where

$$Q = \frac{4\pi\, n \sin(\theta/2)}{\lambda} \quad (4)$$

Here, n is the refractive index of the fluid, λ is the wavelength in the vacuum of the laser light used, and θ is the scattering angle. Therefore, D_f can be estimated from the slope of log I versus log Q.

2.5. Analytical methods

The pH and residual turbidity were directly measured by a pH meter (pH7110, WTW, Germany) and turbidimeter (2100 N, Hach, USA). DOC was measured with a TOC analyzer (Multi N/C 3100, Analytik Jena, Germany). The concentrations of the prepared Al species were measured by an inductively coupled plasma optical emission spectrometer (ICP-OES) (Optima8300, PerkinElmer, USA). The Al-Ferron complexation timed spectrophotometry was used to analyze the Al species distribution of coagulants (Zhou et al., 2006). The fresh flocs after rapid mixing were used for the analysis of Zeta potentials (Zetasizer IV, Malvern, UK). The supernatants with and without filtration over a 0.45 μm membrane were acidified with 0.5 M HNO_3 and injected into the ICP-OES for determination of total and dissolved residual Al. Three-dimensional excitation-emission matrix (3D-EEM) fluorescence spectra of the samples were obtained by Fluorescence Spectrophotometer (FP-6500, Jasco, Japan) with the excitation wavelengths of 220–450 nm and emission wavelengths of 220–500 nm.

3. Results and discussion

3.1. Mutual interactions between MPs and Al species in the MSC process

Based on CCD experiment results (Table SM-3), the RSM was used to establish an empirical relationship between the responses and variables. The rationality of statistical analysis among these reduced quadratic and cubic models was validated with F-test in ANOVA (Table SM-4). The significances of the fitted models between different Al-species ($AlCl_3$, Al_{13}, and Al_{30}) and MPs were validated by the high F-values (59.6–512) and low p-values (<0.0001). The lack of fit (LOF) describes the variations of the data around the adapted model. The large probability of LOF (PLOF > 0.05) indicated that the relationships between response variables and the removal efficiencies were well described by these regression equations (Moghaddam et al., 2010). The ANOVA parameters of these fitted models met all the model requirements ($R^2 > 0.95$, $R^2_{Adj} - R^2_{Pred} < 0.2$, $R^2_{Pred} > 0.7$, and Adeq Precision > 4)

(Wang et al., 2019). The consistency of R^2 values and R^2_{Adj} further showed the reliable predictions of turbidity and DOC removal efficiencies by regression equations. As a measure of the signal to noise ratio, the values of adequate precision (AP) of these fitted models ranged from 22.0 to 57.7. AP values greater than 4 indicated adequate signals for the models within the design space defined by the CCD (Bilici Baskan and Pala 2010). As shown in the diagnostic plots (Fig. SM-2, Fig. SM-3), the satisfactoriness of these models was supported by adequate agreements between predicted versus actual turbidity and DOC removal efficiencies for $AlCl_3$, Al_{13}, and Al_{30}.

Three-dimensional response surface and contour plots were created to illustrate the effects of mutual interactions of two independent variables on pollutants removal (Fig. 1). At a fixed MPs dosage, the turbidity and DOC removal both initially increased with the dose of $AlCl_3$, Al_{13} or Al_{30}, and then decreased with their additional input. As shown in Fig. SM-4, zeta potentials shifted from negative to positive with addition of coagulants. The surface charges reversal and re-stabilization of colloidal particles induced by over-dosage of coagulants led to the deterioration of coagulation performance (Cheng et al., 2008). At fixed doses of Al species, turbidity and DOC removal were also initially increased and then reduced with the excessive addition of MPs. For example, at the Al_{13} dose of 0.064 mM Al, DOC removal was increased from 11.8% to 36.3% as MPs dose increased from 20 to 60 mg L^{-1}, but they then declined to 10.7% as the MPs dose was further increased to 100 mg L^{-1}. This decrease was attributed to the competing consumption of positive charges between MPs and pollutants, as the isoelectric point (IEP) of MPs is at 4.0 for MPs and the MPs would be negatively charged in neutral and alkaline water (Fig. SM-5).

The obvious peaks of response surfaces indicate that the optimal conditions for turbidity and DOC removal were exactly located inside the design boundary, and the corresponding elliptical contour plots showed the significant interactions between Al-species and MPs dosages (Xu et al., 2011b). For turbidity removal, the counter plots of MPs compositing with different Al-species all show considerable curvature, which was decreased as the order of Al_{30} > Al_{13} > $AlCl_3$. These results indicated that MPs seeded coagulation achieved the most significant interactions with the high polymerized Al-species for turbidity removal, especially in the low dosage regions of Al_{30}. For instance, the variation of turbidity removal responding to MPs dosages (20–100 mg L^{-1}) at the Al_{30} dose of 0.09 mM Al (8.6%–69.3%) was more obvious than that at the Al_{30} dose of 0.26 mM Al (88.7%–100%) (Fig. 1e). For DOC removal, the typical elliptic contour plots in Fig. 1d suggested the significant interactive effects between Al_{13} and MPs doses, while the combined response surface of Al_{30} and MPs flattened out (Fig. 1f). In the case of $AlCl_3$, the role of MPs was more pronounced in the regions of higher $AlCl_3$ dosages (>0.16 mM Al) for DOC removal. The influence degree of MPs on DOC removal in different Al species followed the order of Al_{13} > $AlCl_3$ >Al_{30}. Normally, Al_c-DOM complexes can be efficiently separated by gravity due to the high molecular weight of Al_{30}, while some dissolved and colloidal Al_a/Al_b-DOM clusters are too small to be removed by settling (Yan et al., 2008a). Therefore, the successful separation of these small clusters with the coexistence of MPs was inferred to result in the more favorable interactions between MPs and Al_{13}/$AlCl_3$ for DOC removal in the MSC process.

The optimal regions simultaneously satisfied the critical properties of two responses by superimposing the response contours in an overlay plot (Zinatizadeh et al., 2006). Combined with the desired limits for turbidity removal (>95%) and DOC removal

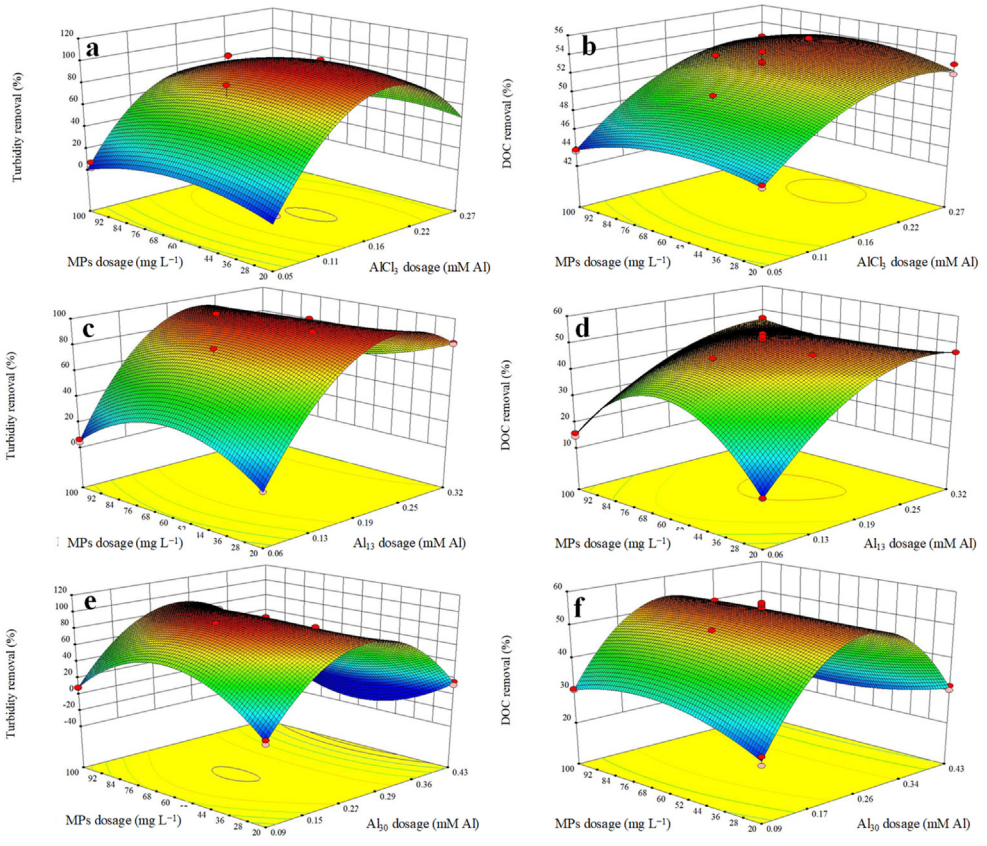

Fig. 1. 3D surface graphs and contour plots of turbidity and DOC removal showing the interactive effects of MPs dosages and Al species dosages: (a, b) $AlCl_3$, (c, d) Al_{13} and (e, f) Al_{30}.

(>50%), the yellow shaded area gives the permissible values of the two variables (Fig. SM-6). The obtained optimal dosages of Al species and MPs for turbidity and DOC removal in the MSC process are summarized in Table SM-5. Verification experiments at the optimum conditions were conducted in triplicates and the obtained results were in good agreement with the prediction with errors ranging from 0.22% to 2.14%.

3.2. Correlations between MPs, Al species and coagulation behavior

3.2.1. Dependence of pollutants removal on MPs and Al species

Turbidity removal using the optimized conditions during MSC and TC jar tests were compared for the three coagulants ($AlCl_3$, Al_{13}, and Al_{30}). In the TC process, the residual turbidity decreased in the order of Al_{13} (1.10 NTU) < Al_{30} (1.35 NTU) < $AlCl_3$ (1.83 NTU) (Fig. 2a). The dominant coagulation flocs of Al species were formed by charge neutralization, and the larger molecular size of Al_{13} and Al_{30} compared to $AlCl_3$ enhanced the aggregating efficiency of these small aggregates by bridging and facilitated the turbidity removal (Yang et al., 2013; Li et al., 2014). The decreased turbidity removal in Al_{30} than Al_{13} could be explained by the existence of Al_a (18.4%) in the coagulant of Al_{30} (Table SM-1). The residual turbidity achieved at different Al species all decreased to less than 1 NTU with MPs addition (41–66 mg L^{-1}), and its descending order was changed to Al_{30} (0.56 NTU) < Al_{13} (0.75 NTU) < $AlCl_3$ (0.81 NTU). The superior turbidity removal in the MSC process compared to the TC process confirmed the effective separation of some colloidal flocs under an applied magnetic field. $AlCl_3$ achieved the most effective DOC removal (52.6%) in the TC process, followed by Al_{30} (51.2%) and Al_{13} (46.8%). The hydrolysis of Al species was confirmed to consume OH− during the coagulation process, and this alkalinity consumption was related to the basicity of Al species (Yan et al., 2008b). The pH values of the coagulated waters declined more obviously with the increase of $AlCl_3$ doses compared to Al_{13} and Al_{30}, which indicated the further hydrolysis of $AlCl_3$ during the coagulation process (Fig. SM-7). Therefore, some small Al_a-DOM clusters could be aggregated to large flocs by the further polymerization of Al_a to in-situ-formed Al_b/Al_c, which was proved to be efficient in DOM removal (Xu et al., 2011c). Some Al_{13}-DOM complexes were not large enough to precipitate compared to those formed by Al_{30}, which led to the low DOC removal in Al_{13}. Compared to the TC process, appreciable improvements of DOC removal were observed with MPs seeding in the MSC process, especially for Al_{13} (from 46.8% to 51.8%). The high charged Al_{13} not only neutralized the negative charged DOM but also acted as the nucleus to produce Al_{13}-DOM complexes in the TC process. Therefore, it was inferred that MPs could serve as nuclei and merge into the formed Al_{13}-DOM complexes, and the effective separation of the produced MPs-Al_{13}-DOM aggregates was responsible for the high DOC removal in MSC process.

Three-dimensional excitation-emission matrix (3D-EEM) fluorescence spectra were used to examine changes in DOM components in the TC and MSC process with different Al species (Fig. 2b). Two apparent EEM peaks at E_x/E_m of 260–275/430–470 nm and 310–360/410–450 nm were classified as humic-like constituents stimulated by UV excitation and visible excitation (Coble 1996). Compared with the spectra of raw water (Fig. SM-8), these two peaks in the treated waters all showed an obvious blue shift and their intensities decreased simultaneously, indicating the reduction of aromatic rings and conjugated bonds of humic-like organic matter by coagulation (Gone et al., 2009; Jin et al., 2016). In the TC process, the intensities of spectra followed the order of $AlCl_3$ < Al_{30} < Al_{13}, which was consistent with the DOC removal efficiencies. Moreover, the intensities of all the fluorescence peaks were significantly decreased with MPs addition, while the peak positions were the same as that of TC (within error E_X < 5 nm, E_m < 10 nm).

3.2.2. Dependence of residual Al distributions on MPs and Al species

The residual Al distributions in the supernatant of the treated water for the determined optimal coagulation conditions are shown in Fig. 3. For both the MSC and TC process, the colloidal Al was dominant in the total Al. The residual colloidal Al and dissolved Al in the TC process exhibited the same tendency following the order of $AlCl_3$ (1.20 mg Al L^{-1}, 0.032 mg Al L^{-1}) > Al_{13} (1.0 mg Al L^{-1},

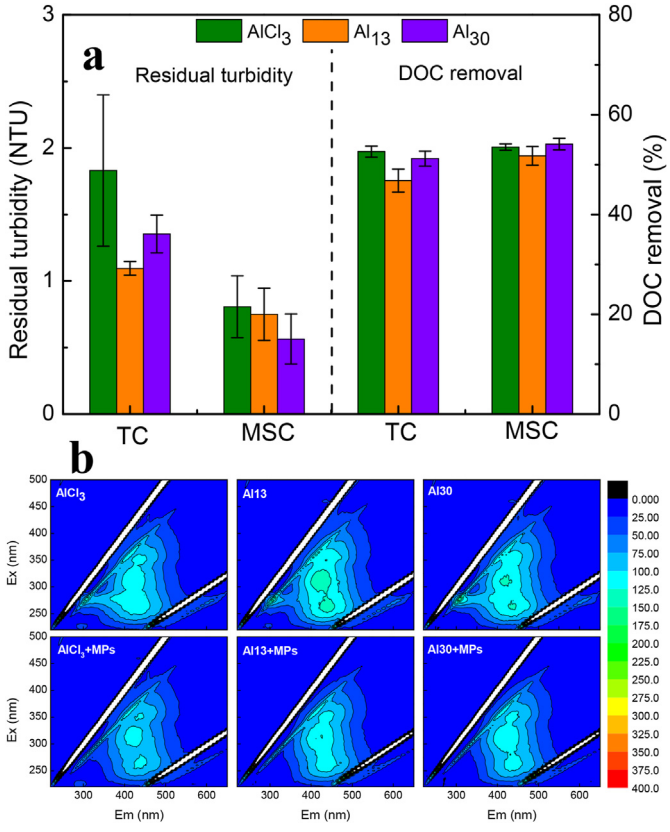

Fig. 2. Dependence of coagulation performance on Al species in the TC and MCF process: (a) turbidity and DOC removal; (b) 3D excitation emission matrix fluorescence spectra of DOM in the supernatant.

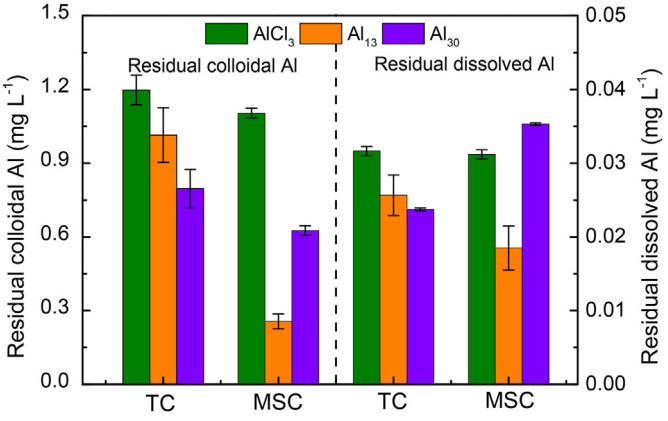

Fig. 3. Dependence of residual Al distributions on Al species in the TC and MCF process.

0.026 mg Al L^{-1}) > Al_{30} (0.80 mg Al L^{-1}, 0.024 mg Al L^{-1}). The higher polymerization degree of Al species led to less residual Al, implying that the precipitable fraction of Al_{30}-induced clusters were more important than the Al_{13}- and $AlCl_3$-induced clusters. The residual colloidal Al and dissolved Al in the MSC process were changed to $AlCl_3$ (1.10 mg Al L^{-1}, 0.031 mg Al L^{-1}), Al_{13} (0.26 mg Al L^{-1}, 0.018 mg Al L^{-1}) and Al_{30} (0.63 mg Al L^{-1}, 0.035 mg Al L^{-1}). For $AlCl_3$, the concentrations of residual Al produced in the MSC and TC process showed no significant differences. Notably, compared to the single addition of Al_{13}, the residual colloidal Al and dissolved Al were significantly reduced by 74.7% and 30.0% with the combined dosing of MPs and Al_{13}, which resulted from the effective settling of the generated MPs-Al_{13}-DOM clusters. For Al_{30}, the colloidal Al was decreased by 0.171 mg L^{-1} with MPs addition, while the dissolved Al was increased by 0.011 mg L^{-1}. Al_{30} is the large polymer formed during aluminum hydrolyzation, which belongs to colloidal or solid Al species. Therefore, the dissolved Al in the treated water of Al_{30} was mainly composed of Al_a or some dissolved Al_a-DOM complexes, while the colloidal Al was closely related to the colloidal Al_a-DOM complexes. The increased residual dissolved Al in Al_{30} suggested that some adsorbed Al_a-DOM complexes were detached from the highly branched flocs of Al_{30} with MPs seeding. Comparing the MSC with the TC process, the total residual Al in the case of Al_{13} achieved the most obvious reduction by 73.6%, followed by Al_{30} (19.5%) and $AlCl_3$ (1.2%).

3.2.3. Dependence of flocs properties on MPs and Al species

The variations of floc properties were closely related to the different coagulation mechanisms. The formation, breakage, and regrowth of aggregates for different Al species in the TC and MSC process were investigated at optimal coagulation conditions (Fig. 4). In the initial steady phase, the average floc sizes (d_{50}) of Al species in the TC process were in the order of $AlCl_3$ (226 μm) > Al_{30} (160 μm) > Al_{13} (152 μm), while that in the MSC process followed the order of $AlCl_3$ (284 μm) > Al_{13} (159 μm) > Al_{30} (141 μm). The coagulation time required for floc size stabilization in the case of $AlCl_3$ and $AlCl_3$+MPs (>7 min) was longer than that in the cases of other Al species (3–5 min). The size distribution of $AlCl_3$-induced flocs of the TC process (ranging from 12.6 to 710 μm) was wider than that of Al_{13}-induced flocs (ranging from 3.2 to 564 μm) and Al_{30}-induced flocs (from 2.8 to 448 μm) (Fig. 5). These results indicated that the formation of small clusters was accompanied by their growth into larger flocs in $AlCl_3$ (Harif et al., 2012). Flocs of $AlCl_3$ could be gradually formed by aggregating Al_a-DOM complexes with in situ formed polynuclear species through the further hydrolyzation of Al_a. With MPs added, the average floc size of $AlCl_3$ was increased by 18.3%. Taking the floc size distribution curve in the TC process as a reference, the increase in the right side of the distribution curve was more obvious than in the left side with MPs addition (Fig. 5a). This phenomenon showed that MPs addition produced larger Al_a-induced clusters by increasing collision efficiencies with more initial particles, and these primary clusters could also be aggregated by interacting with in-situ-formed polynuclear species. For Al_{13}, the average floc size in the TC process was the smallest, which was consistent with the results of Zhao et al., (2010). The whole floc size distribution curve of Al_{13} evenly moved to the right after introducing MPs, which implied the uniform generation of MPs-Al_{13}-DOM complexes (Fig. 5b). For Al_{30}, the adsorption and bridging capacity of the large polymer facilitated the formation of the easily precipitable flocs (Feng et al., 2015). However, the floc size was reduced by 12.0% after introducing MPs into Al_{30} species. The introduction of MPs into Al_{30} led to the decrease of volume percentage of large flocs (180–450 μm) from 50.0% to 37%, and the increase of volume percentage of small flocs (2–180 μm) from 50% to 63% (Fig. 5c). This indicates that some

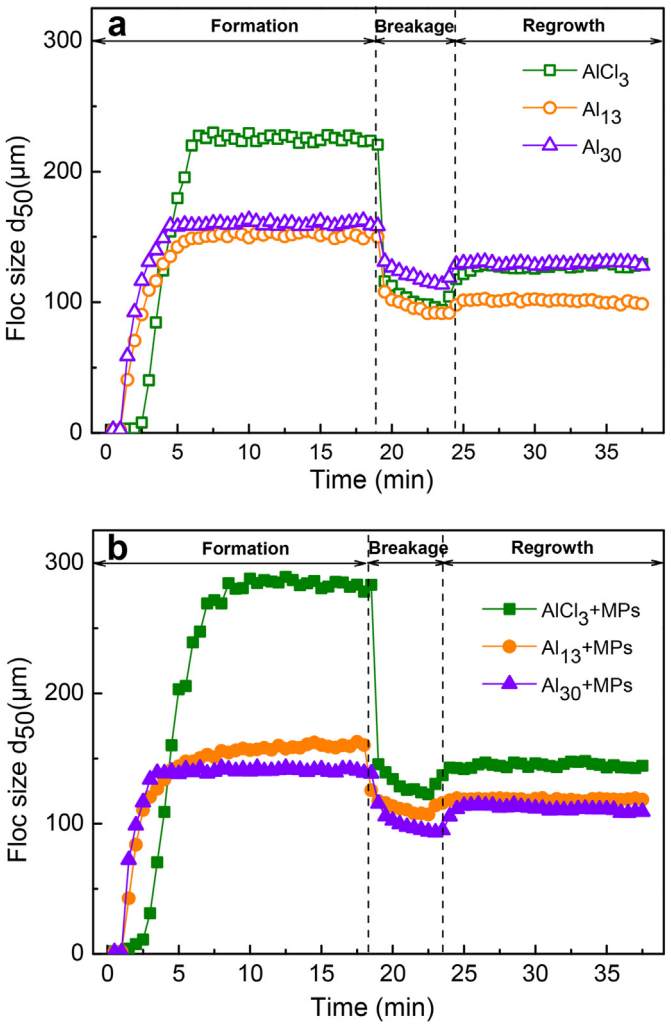

Fig. 4. The flocs formation, breakage and regrowth of $AlCl_3$, Al_{13} and Al_{30} in the TC and MSC process.

fragments detached from the Al_{30} induced flocs after MPs addition.

Once a stable floc size distribution was achieved, the suspensions were exposed to high shear force for 5 min, and then the original slow stirring condition was restored for re-growth of the flocs (Fig. 4). The floc strength factor of $AlCl_3$ (41.8%) was lower than that of Al_{13} (60.3%) and Al_{30} (70.9%) (Table 1). It was confirmed that larger flocs (200–2000 μm) are likely to break up under moderate velocity gradients, whereas flocs smaller than 200 μm are not easily disrupted. (Boller and Blaser 1998). Consistent with the effect of MPs on floc size, the floc strength increased in $AlCl_3$ and Al_{13} with MPs addition, which was reduced in Al_{30} (Table 1). The floc size tended to be stable when the breakage and aggregation of flocs were balanced (Feng et al., 2015). Therefore, the reduced floc strength and floc size by introducing MPs could be attributed to the increased breakages of flocs. MPs addition increased the flocs recovery ability of Al_{13} from 16.1% to 22.5% and Al_{30} from 34.3% to 38.5%.

The variations of floc fractal dimension (D_f) over time were examined for the TC and MSC processes (Fig. SM-9, Table 1). The D_f reflects the openness of the internal floc structure, with a higher value indicating a more compact structure (Ahmad et al., 2008). For different Al species in the TC process, the D_f of flocs followed the order of $AlCl_3$ (2.08) > Al_{13} (1.99) > Al_{30} (1.88). The relatively low D_f values for Al_{13} and Al_{30} were attributed to the highly branched flocs

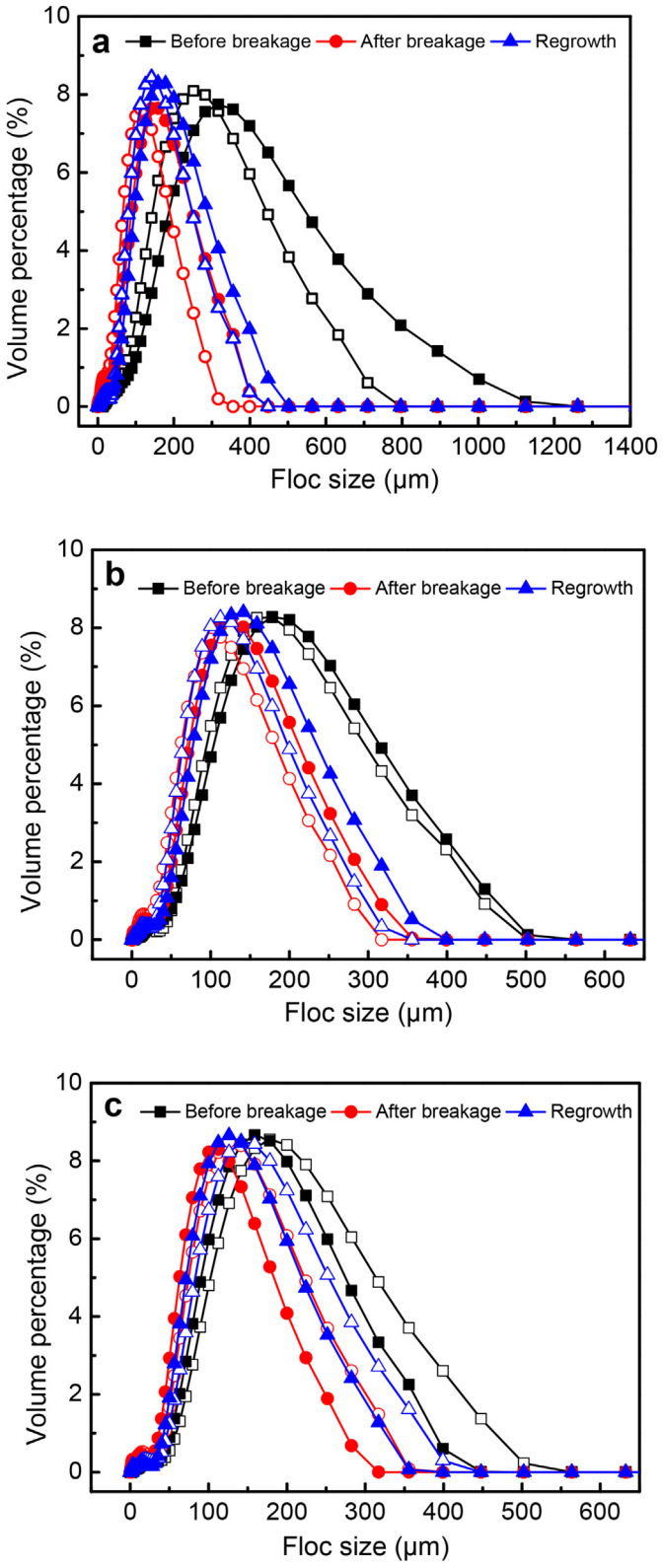

Fig. 5. Size distributions of floc formation, breakage and regrowth for $AlCl_3$, Al_{13} and Al_{30}. (open symbol: TC process; solid symbol: MSC process).

with large and loose bounds. Compared to the transparent and fluffy flocs formed by Al_{13} and Al_{30}, the flocs formed by $AlCl_3$ were indeed more compact and dense. The D_f was reduced by 5.8–22% in the MSC process (Table 1), suggesting the formation of incompact flocs with MPs addition. The images of flocs were in accordance with the results of scattering structural analysis (Fig. 6a). The detachment of partial magnetic clusters from Al_{30} induced-flocs was observed, which was consistent with the decreased flocs strength and size (Fig. 6a and Table 1). In the TC process, D_f values slightly decreased for $AlCl_3$, Al_{13}, and Al_{30} after flocs breakage and regrowth, which was attributed to the broken flocs with fewer potential connection points and more open structures for regrowth than the initial floc growth (Nan et al., 2016).

3.3. Interactive mechanism between MPs and Al species

The proposed interactive mechanisms between MPs and different Al species are shown in Fig. 6b. In general, more hydrophobic components made the affinity of DOM with coagulants stronger than that of kaolin particles (Lv et al., 2018). Negatively charged colloids and particles could be destabilized and aggregated to settable flocs after complete or partial neutralization. Therefore, the interactions between coagulants and dissolved pollutants determined the main residual constituents. Here, DOM as a representative pollutant was used to illustrate the proposed mechanisms.

For $AlCl_3$ in the coagulation process, the obvious decline of the pH of the coagulated water indicated the further polymerization of Al_a to in-situ-formed Al_b/Al_c. The longer time required for floc size stabilization and the wider size distribution of $AlCl_3$-induced clusters than other Al species indicated that the flocs were formed from the aggregation of primary Al_a-DOM complexes with the in-situ-formed Al_b/Al_c. The efficient separation of these large flocs by gravity led to the superior DOC removal, in which interactions between MPs and in-situ formed Al_b would be buried. Negligible changes of dissolved Al after MPs addition suggested the weak connections between the dissolved Al_a-DOM complexes and MPs. Therefore, the decrease of the residual turbidity and colloidal Al with MPs in the $AlCl_3$ coagulation process could be attributed to the effective sedimentation of the formed clusters between MPs and colloidal Al_a-DOM complexes under the applied magnetic field. For Al_{13}, the formed Al_{13}-DOM clusters in the TC process were colloidal or precipitated. MPs seeding evenly increased the floc size across the whole floc size distribution. This indicated that the negatively charged MPs could attach onto high positively charged Al_{13} by charge neutralization, and the MPs and Al_{13} could jointly serve as nuclei for flocs formation. The efficient separation of these aggregated MPs-Al_{13}-DOM complexes could be responsible for the significantly improved removal of DOC and colloidal Al in the MSC process than that in the TC process. Compared to $AlCl_3$ and Al_{13}, using Al_{30} achieved a lower residual Al indicating the production of easily precipitable flocs by adsorption of DOM with high molecular weight polymers. The lowest D_f value of the Al_{30}-induced flocs indicated that the fluffy flocs were formed with the highly branched, large and loose bounds, and some loose fragments with a low specific gravity were detached from the flocs (Fig. 6a). These fragments cannot be easily removed by settling, but they can be removed by filtration. Although looser flocs and more fragments were produced with MPs seeding compared to only coagulation, the applied magnetic field could achieve effective sedimentation of these fragments, leading to the most improved turbidity removal using Al_{30}. The separation of these fragments by filtration during DOC measurements led to little improvement of DOC removal in the MSC process.

4. Conclusions

The results of this study revealed the dependency of coagulation

Table 1
Average size, strength and recovery factors, fractal dimensions of flocs formed from different Al-species at stages of floc formation, breakage and regrowth in the TC and MSC process.

Coagulants	Floc size			S_f (%)	R_f (%)	D_f		
	d_1 (μm)	d_2 (μm)	d_3 (μm)			Formation	Breakage	Regrowth
$AlCl_3$	226	94.2	128	41.8	25.5	2.08	2.07	2.00
Al_{13}	152	91.4	101	60.3	16.1	1.99	1.98	1.94
Al_{30}	160	114	130	70.9	34.3	1.88	1.85	1.85
$AlCl_3$+MPs	284	123	145	43.1	13.7	1.96	1.84	1.83
Al_{13}+MPs	159	107	119	67.5	22.5	1.72	1.65	1.70
Al_{30}+MPs	141	93.3	112	66.1	38.5	1.60	1.47	1.55

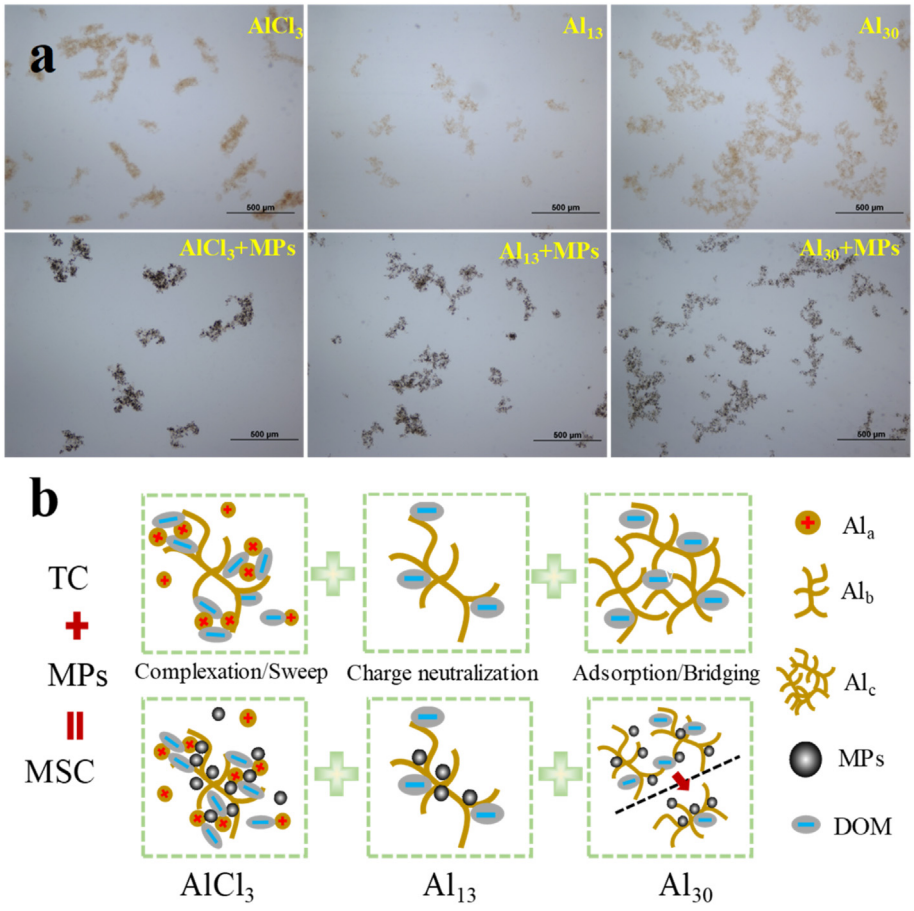

Fig. 6. Coagulation (a) floc images and (b) concept models of $AlCl_3$, Al_{13} and Al_{30} in the TC and MSC process.

behavior on the interactions between different Al species and MPs. Integrating MPs into the floc growth of $AlCl_3$ increased the size of the flocs from 226 to 284 μm by facilitating the formation of large primary clusters and their aggregation with the in-situ-formed Al_b, which was beneficial to increase the handling capacity of the MSC process compared to the TC process. The formation of MPs-Al_{13}-DOM clusters during the MSC process of compositing Al_{13} with MPs played the most significant role in improving DOC removal by 10.7% and reducing residual Al by 73.6%. The most significant interactions between MPs and Al_{30} were observed for turbidity removal, in which the residual turbidity decreased from 1.35 to 0.56 NTU after MPs addition. This was attributed to the effective sedimentation of detached fragments under an applied magnetic field. Considering the specific requirement for enhanced pollutants removal in the MSC process, this study guides the application of Al-based coagulants to match the treatment of various raw water.

Credit author statement

Miao Lv: Conceptualization, Data curation, Formal analysis, Writing – original draft. Dongyi Li: Data curation, Zhaohan Zhang: Supervision, Funding acquisition. Bruce E. Logan: Writing – review & editing, Jan Peter van der Hoek- Review & Editing, Muchen Sun: Visualization, Investigation. Fan Chen: Visualization. Yujie Feng: Supervision, Project administration.

Declaration of competing interest

The authors declare that they have no known competing financial interests or personal relationships that could have

appeared to influence the work reported in this paper.

Acknowledgements

This research was supported by National Key Research and Development Program of China (2016YFC0401106), Heilongjiang Province Natural Science Foundation (No. LH2019E042), State Key Laboratory of Urban Water Resource and Environment, Harbin Institute of Technology (No. 2019TS06), and National Natural Science Foundation of China (21972036). The authors also acknowledged the support of the Innovation Team in Key Areas of the Ministry of Science and Technology.

Appendix A. Supplementary data

Supplementary data to this article can be found online at https://doi.org/10.1016/j.chemosphere.2020.129363.

References

Ahmad, A.L., Chong, M.F., Bhatia, S., 2008. Population Balance Model (PBM) for flocculation process: simulation and experimental studies of palm oil mill effluent (POME) pretreatment. Chem. Eng. J. 140 (1), 86–100.
Ambashta, R.D., Sillanpää, M., 2010. Water purification using magnetic assistance: a review. J. Hazard Mater. 180 (1), 38–49.
Bilici Baskan, M., Pala, A., 2010. A statistical experiment design approach for arsenic removal by coagulation process using aluminum sulfate. Desalination 254 (1), 42–48.
Boller, M., Blaser, S., 1998. Particles under stress. Water Sci. Technol. 37 (10), 9–29.
Cao, B., Gao, B., Wang, M., Sun, X., Wang, J., 2015. Floc properties of polyaluminum ferric chloride in water treatment: the effect of Al/Fe molar ratio and basicity. J. Colloid Interface Sci. 458, 247–254.
Cheng, W.P., Chi, F.H., Li, C.C., Yu, R.F., 2008. A study on the removal of organic substances from low-turbidity and low-alkalinity water with metal-polysilicate coagulants. Colloids Surf., A 312 (2), 238–244.
Coble, P.G., 1996. Characterization of marine and terrestrial DOM in seawater using excitation-emission matrix spectroscopy. Mar. Chem. 51 (4), 325–346.
Duan, S., Xu, H., Xiao, F., Wang, D., Ye, C., Jiao, R., Liu, Y., 2014. Effects of Al species on coagulation efficiency, residual Al and floc properties in surface water treatment. Colloids Surf., A 459, 14–21.
Feng, L., Wang, W., Feng, R., Zhao, S., Dong, H., Sun, S., Gao, B., Yue, Q., 2015. Coagulation performance and membrane fouling of different aluminum species during coagulation/ultrafiltration combined process. Chem. Eng. J. 262, 1161–1167.
Ferhat, M., Kadouche, S., Lounici, H., 2016. Immobilization of heavy metals by modified bentonite coupled coagulation/flocculation process in the presence of a biological flocculant. Desalin. Water Treat. 57 (13), 6072–6080.
Gao, B., Chu, Y., Yue, Q., Wang, Y., 2009. Purification and characterization of Al_{13} species in coagulant polyaluminum chloride. J. Environ. Sci. 21 (1), 18–22.
Gauthier, E., Fortier, I., Courchesne, F., Pepin, P., Mortimer, J., Gauvreau, D., 2000. Aluminum forms in drinking water and risk of Alzheimer's disease. Environ. Res. 84 (3), 234–246.
Gone, D.L., Seidel, J.L., Batiot, C., Bamory, K., Ligban, R., Biemi, J., 2009. Using fluorescence spectroscopy EEM to evaluate the efficiency of organic matter removal during coagulation–flocculation of a tropical surface water (Agbo reservoir). J. Hazard Mater. 172 (2), 693–699.
Harif, T., Khai, M., Adin, A., 2012. Electrocoagulation versus chemical coagulation: coagulation/flocculation mechanisms and resulting floc characteristics. Water Res. 46 (10), 3177–3188.
Hu, C., Liu, H., Chen, G., Qu, J., 2012. Effect of aluminum speciation on arsenic removal during coagulation process. Separ. Purif. Technol. 86, 35–40.
Huangfu, X., Ma, C., Ma, J., He, Q., Yang, C., Jiang, J., Wang, Y., Wu, Z., 2017. Significantly improving trace thallium removal from surface waters during coagulation enhanced by nanosized manganese dioxide. Chemosphere 168, 264–271.
Ibarra-Rodríguez, D., Lizardi-Mendoza, J., López-Maldonado, E.A., Oropeza-Guzmán, M.T., 2017. Capacity of 'nopal' pectin as a dual coagulant-flocculant agent for heavy metals removal. Chem. Eng. J. 323, 19–28.
Jiang, C., Wang, R., Ma, W., 2010. The effect of magnetic nanoparticles on Microcystis aeruginosa removal by a composite coagulant. Colloids Surf., A 369 (1), 260–267.
Jin, P., Jin, X., Bjerkelund, V.A., Østerhus, S.W., Wang, X.C., Yang, L., 2016. A study on the reactivity characteristics of dissolved effluent organic matter (EfOM) from municipal wastewater treatment plant during ozonation. Water Res. 88, 643–652.
Lapointe, M., Barbeau, B., 2018. Selection of media for the design of ballasted flocculation processes. Water Res. 147, 25–32.
Lee, K.E., Morad, N., Teng, T.T., Poh, B.T., 2012. Development, characterization and the application of hybrid materials in coagulation/flocculation of wastewater: a review. Chem. Eng. J. 203, 370–386.
Li, R., Gao, B., Huang, X., Dong, H., Li, X., Yue, Q., Wang, Y., Li, Q., 2014. Compound bioflocculant and polyaluminum chloride in kaolin-humic acid coagulation: factors influencing coagulation performance and floc characteristics. Bioresour. Technol. 172, 8–15.
Liao, Z.L., Chen, H., Zhu, B.R., Li, H.Z., 2016. Analysis and selection of powdered zeolite dosing point in enhanced coagulation–sedimentation for treating micro ammonia polluted raw water. Desalin. Water Treat. 57 (5), 2142–2151.
Lin, J.L., Chin, C.J.M., Huang, C., Pan, J.R., Wang, D., 2008. Coagulation behavior of Al_{13} aggregates. Water Res. 42 (16), 4281–4290.
Liu, J., Cheng, S., Cao, N., Geng, C., He, C., Shi, Q., Xu, C., Ni, J., DuChanois, R.M., Elimelech, M., Zhao, H., 2019. Actinia-like multifunctional nanocoagulant for single-step removal of water contaminants. Nat. Nanotechnol. 14 (1), 64–71.
Lv, D., Zheng, L., Zhang, H., Deng, Y., 2018. Coagulation of colloidal particles with ferrate(vi). Environ. Sci.: Water Res. Technol. 4 (5), 701–710.
Lv, M., Zhang, Z., Zeng, J., Liu, J., Sun, M., Yadav, R.S., Feng, Y., 2019. Roles of magnetic particles in magnetic seeding coagulation-flocculation process for surface water treatment. Separ. Purif. Technol. 212, 337–343.
Mandel, K., Hutter, F., Gellermann, C., Sextl, G., 2013. Reusable superparamagnetic nanocomposite particles for magnetic separation of iron hydroxide precipitates to remove and recover heavy metal ions from aqueous solutions. Separ. Purif. Technol. 109, 144–147.
Moghaddam, S.S., Moghaddam, M.A., Arami, M., 2010. Coagulation/flocculation process for dye removal using sludge from water treatment plant: optimization through response surface methodology. J. Hazard Mater. 175 (1–3), 651–657.
Nan, J., Yao, M., Chen, T., Wang, Z., Li, Q., Zhan, D., 2016. Experimental and numerical characterization of floc morphology: role of changing hydraulic retention time under flocculation mechanisms. Environ. Sci. Pollut. Res. 23 (4), 3596–3608.
Shirasaki, N., Matsushita, T., Matsui, Y., Marubayashi, T., 2016. Effect of aluminum hydrolyte species on human enterovirus removal from water during the coagulation process. Chem. Eng. J. 284, 786–793.
Simate, G.S., Iyuke, S.E., Ndlovu, S., Heydenrych, M., 2012. The heterogeneous coagulation and flocculation of brewery wastewater using carbon nanotubes. Water Res. 46 (4), 1185–1197.
Song, S., Lopez-Valdivieso, A., Hernandez-Campos, D.J., Peng, C., Monroy-Fernandez, M.G., Razo-Soto, I., 2006. Arsenic removal from high-arsenic water by enhanced coagulation with ferric ions and coarse calcite. Water Res. 40 (2), 364–372.
Su, Z., Liu, T., Yu, W., Li, X., Graham, N.J.D., 2017. Coagulation of surface water: observations on the significance of biopolymers. Water Res. 126, 144–152.
Wan, T.J., Shen, S.M., Siao, S.H., Huang, C.F., Cheng, C.Y., 2011. Using magnetic seeds to improve the aggregation and precipitation of nanoparticles from backside grinding wastewater. Water Res. 45 (19), 6301–6307.
Wang, N., Li, X., Yang, Y., Shang, Y., Zhuang, X., Li, H., Zhou, Z., 2019. Combined process of visible light irradiation photocatalysis-coagulation enhances natural organic matter removal: optimization of influencing factors and mechanism. Chem. Eng. J. 374, 748–759.
Wu, C.D., Xu, X.J., Liang, J.L., Wang, Q., Dong, Q., Liang, W.L., 2011. Enhanced coagulation for treating slightly polluted algae-containing surface water combining polyaluminum chloride (PAC) with diatomite. Desalination 279 (1), 140–145.
Xu, J., Sheng, G.P., Luo, H.W., Fang, F., Li, W.W., Zeng, R.J., Tong, Z.H., Yu, H.Q., 2011b. Evaluating the influence of process parameters on soluble microbial products formation using response surface methodology coupled with grey relational analysis. Water Res. 45 (2), 674–680.
Xu, L., Guo, C., Wang, F., Zheng, S., Liu, C.Z., 2011a. A simple and rapid harvesting method for microalgae by in situ magnetic separation. Bioresour. Technol. 102 (21), 10047–10051.
Xu, W., Gao, B., Wang, Y., Yang, Z., Bo, X., 2011c. Role of Al_{13} species in removal of natural organic matter from low specific UV absorbance surface water and the aggregates characterization. Chem. Eng. J. 171 (3), 926–934.
Xu, W., Gao, B., Yue, Q., Wang, Y., 2010. Effect of shear force and solution pH on flocs breakage and re-growth formed by nano-Al_{13} polymer. Water Res. 44 (6), 1893–1899.
Xue, N., Wang, X., Zhang, F., Wang, Y., Chu, Y., Zheng, Y., 2016. Effect of SiO_2 nanoparticles on the removal of natural organic matter (NOM) by coagulation. Environ. Sci. Pollut. Res. 23 (12), 11835–11844.
Yan, M., Wang, D., Ni, J., Qu, J., Chow, C.W., Liu, H., 2008a. Mechanism of natural organic matter removal by polyaluminum chloride: effect of coagulant particle size and hydrolysis kinetics. Water Res. 42 (13), 3361–3370.
Yan, M., Wang, D., Qu, J., He, W., Chow, C.W.K., 2007. Relative importance of hydrolyzed Al(III) species (Al_a, Al_b, and Al_c) during coagulation with polyaluminum chloride: a case study with the typical micro-polluted source waters. J. Colloid Interface Sci. 316 (2), 482–489.
Yan, M., Wang, D., Yu, J., Ni, J., Edwards, M., Qu, J., 2008b. Enhanced coagulation with polyaluminum chlorides: role of pH/alkalinity and speciation. Chemosphere 71 (9), 1665–1673.
Yang, Z., Liu, B., Gao, B., Wang, Y., Yue, Q., 2013. Effect of Al species in polyaluminum silicate chloride (PASiC) on its coagulation performance in humic acid–kaolin synthetic water. Separ. Purif. Technol. 111, 119–124.
Yang, Z.L., Gao, B.Y., Yue, Q.Y., Wang, Y., 2010. Effect of pH on the coagulation performance of Al-based coagulants and residual aluminum speciation during the treatment of humic acid–kaolin synthetic water. J. Hazard Mater. 178 (1), 596–603.
Yao, M., Nan, J., Chen, T., 2014. Effect of particle size distribution on turbidity under various water quality levels during flocculation processes. Desalination 354, 116–124.

Ye, C., Bi, Z., Wang, D., 2013. Formation of Al30 from aqueous polyaluminum chloride under high temperature: role of Al_{13} aggregates. Colloids Surf., A 436, 782–786.
Zhang, M., Xiao, F., Xu, X.Z., Wang, D.S., 2012. Novel ferromagnetic nanoparticle composited PACls and their coagulation characteristics. Water Res. 46 (1), 127–135.
Zhao, B., Wang, D., Li, T., Chow, C.W.K., Huang, C., 2010. Influence of floc structure on coagulation–microfiltration performance: effect of Al speciation characteristics of PACls. Separ. Purif. Technol. 72 (1), 22–27.
Zhou, W., Gao, B., Yue, Q., Liu, L., Wang, Y., 2006. Al-Ferron kinetics and quantitative calculation of Al(III) species in polyaluminum chloride coagulants. Colloids Surf., A 278 (1), 235–240.
Zinatizadeh, A.A.L., Mohamed, A.R., Abdullah, A.Z., Mashitah, M.D., Hasnain Isa, M., Najafpour, G.D., 2006. Process modeling and analysis of palm oil mill effluent treatment in an up-flow anaerobic sludge fixed film bioreactor using response surface methodology (RSM). Water Res. 40 (17), 3193–3208.